Electronic Supplementary Material (ESI) for Journal of Materials Chemistry C.

Supporting Information

Versatile robust organogels based on low molecular weight gelator of phenylquinolinylacrylonitrile

Cheng Liu, Kaiqi Ye*, Huan Xiao, Yuan Yue, Jingbo Sun, and Ran Lu*

Sate Key Laboratory of Supramolecular Structure and Materials, College of Chemistry, Jilin University, Changchun, China.

E-mail: yekq@jlu.edu.cn; luran@mail.jlu.edu.cn

EXPERIMENTAL SECTION

General Information

The regents were commercially available and used as supplied without purification. ^{1}H NMR and ^{13}C NMR spectra were recorded with a Bruker-Avance III 400 MHz and 101 MHz spectrometers with $CDCl_3$ and DMSO-d_6 as solvents and tetramethylsilane (TMS) as the internal standard. The samples for irradiation time-dependent ^{1}H NMR measurements were gained via the irradiation of the solution, gels or crystals of **1**, **2** and **3** by 365 nm (16.7 mW/cm^2) light for different times, followed by removing the solvent and then dissolving in DMSO-d_6 or directly dissolving in DMSO-d_6. FT-IR spectra were obtained with a Nicolet-360 FT-IR spectrometer by the incorporation of samples into KBr disks. HPLC-MS was measured on Bruker esquire HCT apparatus. UV-vis absorption spectra were measured by a Shimadzu UV-1601PC spectrophotometer. Fluorescence emission spectra were taken on a Shimadzu RF-5301 luminescence spectrometer. X-ray diffraction patterns were obtained on Empyrean XRD equipped with graphite monochromatized Cu-Kα radiation (λ = 1.5418 Å) employing a scanning rate of 0.00267 °/s in the 2θ range of 5° to 40° and the samples were kept at room temperature during data collection. Single crystals of **2** and **3** were selected for single crystal X-ray diffraction analysis on a Rigaku RAXIS-RA PID diffractometer using graphite-monochromated MoK_α radiation (λ = 0.71073 Å), and the crystals were kept at room temperature during data collection. The structures were solved by the direct methods and refined on F2 by full-matrix least-square using the SHELXTL-97 program. Scanning electron microscopy (SEM) was performed on a HITACHI SU8020 (operating at 3 kV). The xerogels were placed on silica wafer and coated with gold for SEM measurements. Rheological measurements were performed on a TA instrument (AR2000 Rheometer) equipped with an aluminum plate of 8 mm diameter. The samples were sandwiched between the two plates with a gap of 1.0 mm throughout the experiments.

Preparation of organogels and xerogel films

The preparation of organogels were according to the previous precedure.[2,3] The hot solutions of **2** or **3** in acetone/water (v/v = 1/1) were sonicated first for several seconds and then cooled naturally until organogels were formed. After the acetone/water organogels of **2** and **3** were dispersed into *n*-hexane, the well-dispersed nanofibers were produced. The xerogel films were prepared after casting the nanofibers onto the substrates, followed by the evaporation of the solvent naturally.

Preparation of the free-standing organogels (FSOG) and free-standing hydrogels (FSHG)

The hot acetone/water (v/v = 1/1) solutions of **2** (12 mg) and ink (1 μL) were sonicated first for several seconds and then cooled naturally until the organogels formed. The formed organogels were removed from the test tube or cuvette to give the free-standing organogels, which could be immersed in water for hours to give FSHG.

Sensory properties investigation

The sensory properties for the xerogel films were carried out at 25 °C. Firstly, the acid vapors at a certain concentration were obtained by diluting the saturated vapors with nitrogen, and then were injected into a quartz cell (10 mm in width) containing the film. The changes in the emission were recorded after the injection of acid vapor for 10 s.

UV irradiation of self-standing organogel

The upper part of the free-standing organogel was threaded with a needle, which was fixed with brackets, and was irradiated by LED lamp (365 nm, 16.7 mW/cm^2). The process was recorded by Mi 10S.

Synthesis

(*Z*)-2-phenyl-3-(quinolin-4-yl)acrylonitrile (**1**)

Sodium hydroxide (0. 06 g, 1.53 mmol) was dissolved in ethanol (30 mL) in a 100 mL round bottom flask. Quinoline-4-carbaldehyde (0.2 g, 1.27 mmol) was added subsequently. After that, 2-phenylacetonitrile (0.18 g, 1.53 mmol) in ethanol (10 mL) was added dropwise. After stirred at room temperature overnight, the crude product was collected via filtration over a Buchner funnel. And then, the filter cake was added

in dichloromethane under stirring. The precipitation was removed by filtration. Subsequently, petroleum ether (6 times of V_{DCM}) was added gradually into the saturated dichloromethane solution, and the yellow solid was collected (0.16 g, yield is 48%). Mp: 114.0-116.0 °C; ^{1}H NMR (400 MHz, DMSO-d_6) δ 9.07 (d, J = 4.4 Hz, 1H), 8.78 (s, 1H), 8.25 (d, J = 8.4 Hz, 1H), 8.14 (d, J = 8.4 Hz, 1H), 7.96 – 7.86 (m, 4H), 7.73 (t, J = 7.6 Hz, 1H), 7.62-7.53 (m, 3H) (Figure S32); ^{13}C NMR (101 MHz, $CDCl_3$) δ 150.30, 148.38, 139.21, 137.03, 133.26, 130.51, 130.36, 130.00, 129.37, 127.53, 126.45, 126.09, 123.25, 120.16, 118.70, 116.69 (Figure S33); FT-IR (KBr, cm^{-1}): 3423.4, 3060.0, 3028.8, 3002.7, 2220.1, 1615.2, 1582.1, 1562.3, 1505.3, 1450.9, 1387.6, 1361.4, 1342.9, 1267.1, 1250.9, 1161.3, 1143.5, 1081.3, 1000.6, 955.6, 895.7, 867.8, 848.1, 813.4, 765.7, 747.4, 687.8, 594.5, 527.9, 483.3, 465.8, 435.7; HPLC-MS: Calcd. For $C_{18}H_{12}N_2$ 257.1080, found: 257.1068 $[M+H]^+$ (Figure S34).

(*Z*)-2-(4-fluorophenyl)-3-(quinolin-4-yl)acrylonitrile (**2**)

Compound **2** was prepared according to a similar synthetic method as that for compound **1** from quinoline-4-carbaldehyde (0.2 g, 1.27 mmol), 2-(4-fluorophenyl)acetonitrile (0.21 g, 1.53 mmol) and sodium hydroxide (0. 06 g, 1.53 mmol). After stirred at room temperature for 6 h, the reaction mixture was poured into water (200 mL). The crude product was collected via filtration over a Buchner funnel. And then, the filter cake was added in dichloromethane under stirring. The precipitation was removed by filtration. Subsequently, petroleum ether (5 times of V_{DCM}) was added gradually into the saturated dichloromethane solution, and the yellow solid was collected (0.17 g, yield is 52%). Mp: 118.0-120.0 °C; ^{1}H NMR (400 MHz, DMSO-d_6) δ 9.07 (d, J = 4.8 Hz, 1H), 8.76 (s, 1H), 8.25 (d, J = 8.4 Hz, 1H), 8.14 (d, J = 8.4 Hz, 1H), 8.01 (dd, J = 8.8, 5.2 Hz, 2H), 7.92 – 7.86 (m, 2H), 7.72 (t, J = 7.2 Hz, 1H), 7.45 (t, J = 8.8 Hz, 2H) (Figure S35); ^{13}C NMR (101 MHz, $CDCl_3$) δ 163.86 (d, J = 253.1 Hz), 150.30, 148.40, 139.01, 136.90, 130.56, 130.04, 129.47 (d, J = 3.3 Hz), 128.44 (d, J = 8.6 Hz), 127.57, 126.02, 123.17, 120.12, 117.57, 116.56, 116.54 (d, J = 22.2 Hz) (Figure S36); FT-IR (KBr, cm^{-1}): 3048.5, 2216.6, 1603.2, 1582.2, 1564.8, 1511.9, 1463.6, 1424.6, 1389.7, 1360.1, 1307.4, 1258.1, 1253.8, 1235.8, 1212.6, 1165.1, 1151.4, 1013.9, 903.2, 874.6, 841.7, 793.9, 776.1, 754.5, 619.8, 571.9, 505.5, 457.5,

442.4; HPLC-MS: Calcd. For $C_{18}H_{11}FN_2$ 275.0906, found: 275.0973 $[M+H]^+$ (Figure S37).

(*Z*)-3-(quinolin-4-yl)-2-(4-(trifluoromethyl)phenyl)acrylonitrile (**3**)

Compound **3** was prepared according to a similar synthetic method as that for compound **1** from quinoline-4-carbaldehyde (0.2 g, 1.27 mmol), 2-(4-(trifluoromethyl)phenyl)acetonitrile (0.28 g, 1.53 mmol) and sodium hydroxide (0.06 g, 1.53 mmol). After stirred at room temperature for 8 h, the crude product was collected via filtration over a Buchner funnel. The purification of compound **3** was same as that for compound **1**. The yellow solid (0.17 g, yield is 42%) was gained. Mp: 128.0-131.0 °C; ^{1}H NMR (400 MHz, DMSO-d_6) δ 9.09 (d, J = 4.4 Hz, 1H), 8.95 (s, 1H), 8.27 (d, J = 8.4 Hz, 1H), 8.16 (t, J = 7.6 Hz, 3H), 7.98 – 7.95 (m, 3H), 7.89 (t, J = 8.0 Hz, 1H), 7.73 (t, J = 8.0 Hz, 1H) (Figure S38); ^{13}C NMR (101 MHz, $CDCl_3$) δ 150.26, 148.41, 139.29, 138.58, 136.60, 132.35 (t, J = 33.5 Hz), 130.41 (d, J = 45.7 Hz), 127.77, 126.85, 126.40 (d, J = 3.7 Hz), 125.86, 124.99, 123.05, 122.28, 120.16, 117.42, 116.17 (Figure S39); FT-IR (KBr, cm^{-1}): 3072.5, 3054.7, 3011.8, 2216.4, 1616.3, 1580.7, 1563.3, 1504.3, 1461.6, 1415.0, 1389.8, 1323.4, 1242.5, 1178.5, 1141.8, 1118.4, 1069.0, 1016.1, 988.8, 968.6, 915.9, 871.5, 846.1, 836.3, 794.1, 776.0, 758.5, 731.2, 677.9, 602.2, 517.3, 494.8, 454.3, 431.2; HPLC-MS: Calcd. For $C_{19}H_{11}F_3N_2$ 325.0954, found: 325.0932 $[M+H]^+$ (Figure S40).

Table S1. Main electronic transitions calculated with TD-DFT.

Compound	λ_{abs}[a] (nm)	λ_{abs}[b] (nm)	f [c]	Main Transition [d]
	214	221.45	0.0388	H→L+4
1	257	254.73	0.0147	H-2→L+1
	325	310.10	0.1719	H-1→L
	216	213.73	0.0773	H→L+4
2	260	252.05	0.1064	H-5→L
	323	335.85	0.2059	H-2→L
	216	224.15	0.2111	H→L+3
3	263	267.25	0.0182	H→L+1
	328	329.78	0.3488	H-2→L

[a] Experimental absorption in cyclohexane; [b] Calculated absorption in cyclohexane;

[c] Oscillator strength; [d] H represents HOMO, L represents LUMO.

Table S2. Gelation abilities of **1**, **2** and **3** in selected organic solvents.

Solvent	**1** (CGC)	**2** (CGC)	**3**
Petroleum ether	P	I	I
Ethanol	G (2.53)	S	S
Ethyl acetate	S	S	S
i-Propanol	G (2.55)	P	P
1,2-Dichloroethane	S	S	S
Toluene	S	S	S
1,4-Dioxane	S	S	S
Acetonitrile	G (2.54)	S	S
Acetone	S	S	S
Acetonitrile/H_2O	G (0.75, v/v = 1/1)	G (0.53, v/v = 1/3)	S
Acetone/H_2O	G (0.38, v/v = 1.4/1)	G (0.11, v/v = 1/1.3)	P

G: gel, S: solution, P: precipitate, I: insoluble, CGC: critical gelation concentration (wt%)

Table S3. Single crystal data and structure refinement for **2**, **3**, **4** and **5**.

	2	**3**	**4**	**5**
Formula	$C_{18}H_{11}FN_2$	$C_{19}H_{11}F_3N_2$	$C_{18}H_9FN_2$	$C_{18}H_{10}N_2$
Formula weight	274.29	324.30	272.27	254.28
Space group	$P2_1/c$	P-1	P-1	$C2/c$
Crystal system	monoclinic	triclinic	triclinic	monoclinic
a/Å	7.2368(6)	6.9801(7)	3.7431(7)	29.4976(15)
b/Å	5.0575(4)	9.2324(9)	12.294(3)	4.2990(2)
c/Å	36.437(3)	12.0514(13)	14.717(3)	19.9989(10)
α/deg	90	84.242(4)	88.588(12)	90
β/deg	95.354(3)	86.465(4)	88.971(8)	104.202(2)
γ/deg	90	76.598(4)	87.456(7)	90
Volume/ Å^3	1327.78(19)	751.08(13)	676.3(2)	2458.6(2)
Z	4	2	2	8
D(calc)/g cm^{-3}	1.372	1.434	1.337	1.374
μ/mm^{-1}	0.092	0.112	0.090	0.082
Final R indexes	R_1 = 0.1067	R_1 = 0.0466	R_1 = 0.0462	R_1 = 0.0433
[I>2sigma(I)]	wR_2 = 0.2113	wR_2 = 0.1152	wR_2 = 0.1282	wR_2 = 0.1147
R indexes (all	R_1 = 0.1237	R_1 = 0.0569	R_1 = 0.0689	R_1 = 0.0638
data)	wR_2 = 0.2173	wR_2 = 0.1218	wR_2 = 0.1431	wR_2 = 0.1320
GoF	1.253	1.053	1.046	1.055
CCDC	2214985	2214984	2214983	2214982

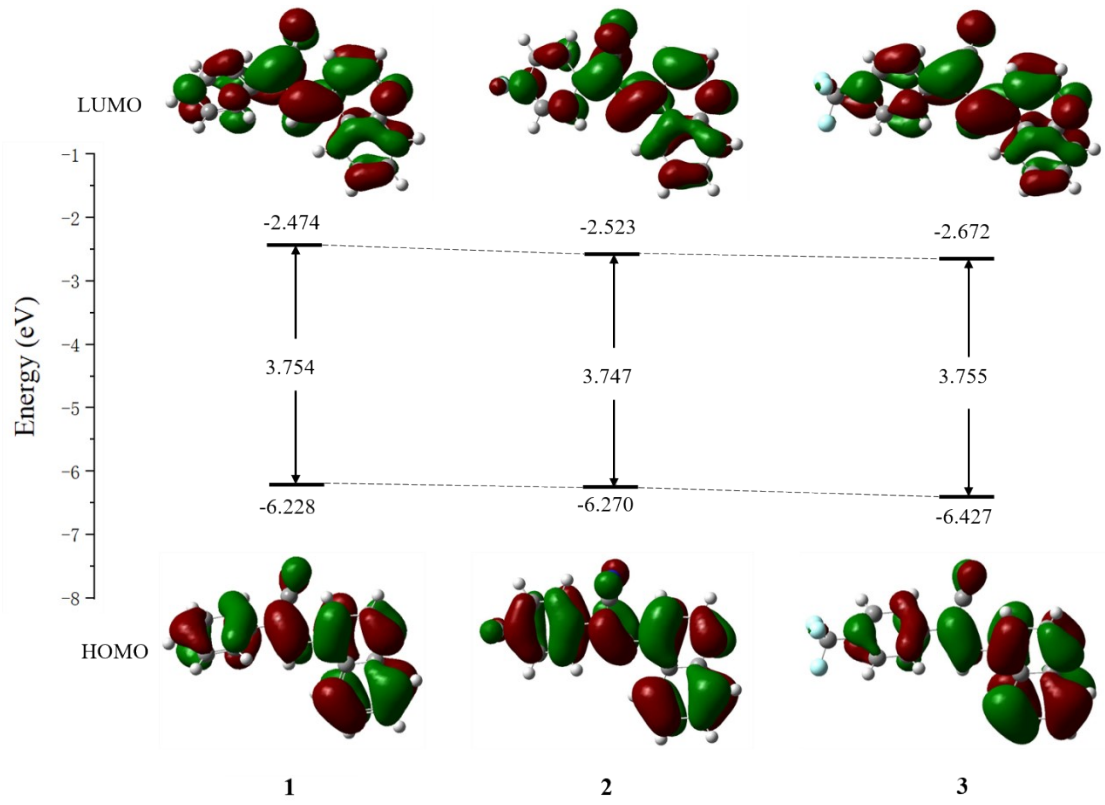

Figure S1. The frontier molecular orbital plots and energy levels for the HOMOs and LUMOs of **1**, **2** and **3**.

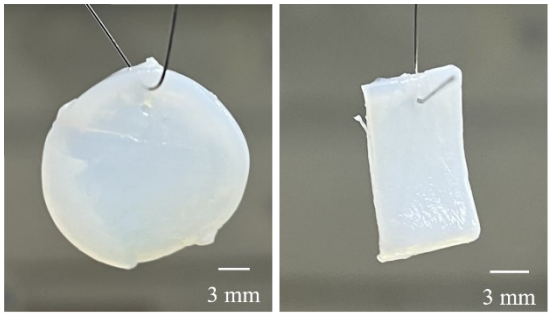

Figure S2. Photos of free-standing organogel (FSOG, 0.56 wt%) based on **2** with different shape obtained from the different mold.

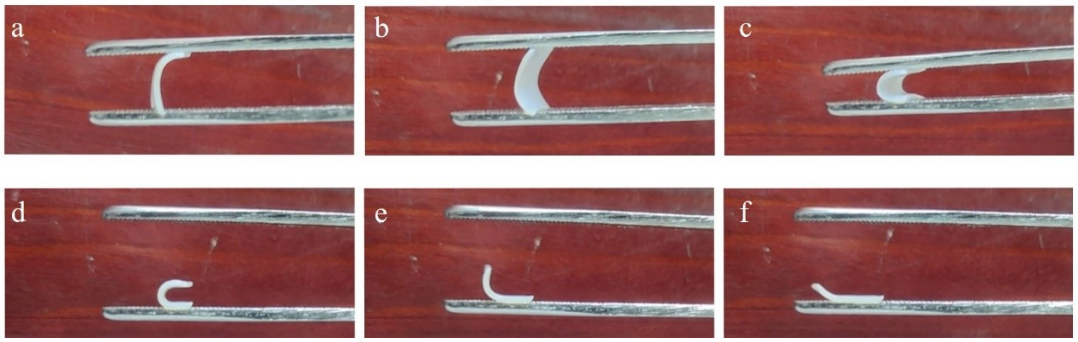

Figure S3. Photos in the process of the mechanical deformation of the FSOG (0.74 wt%, $v_{acetone}/v_{water}$ = 1/1) based on **2** under external mechanical force.

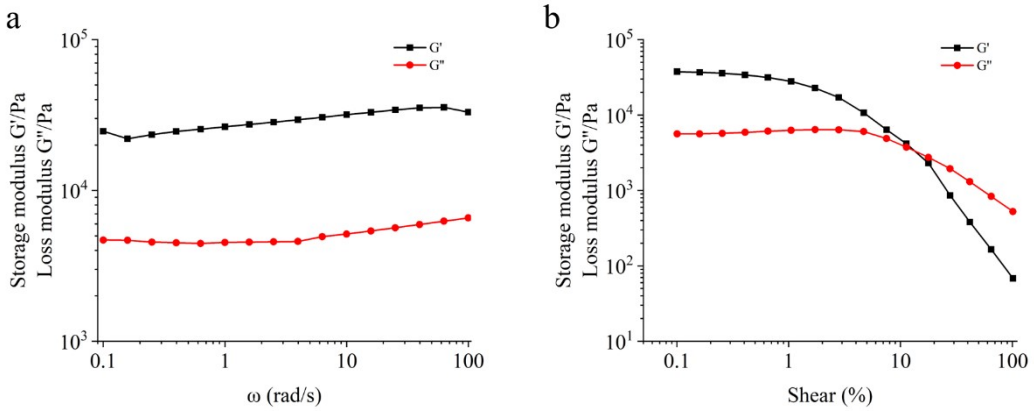

Figure S4. (a) Frequency dependence of storage modulus (G′) and loss modulus (G″) of FSOG based on **2** (0.74 wt%, $v_{acetone}/v_{water}$ = 1/1, strain: 0.1%); (b) Shear dependence of G′ and G″ of FSOG based on **2** (0.74 wt%, $v_{acetone}/v_{water}$ = 1/1, angular frequency at 5 rad/s).

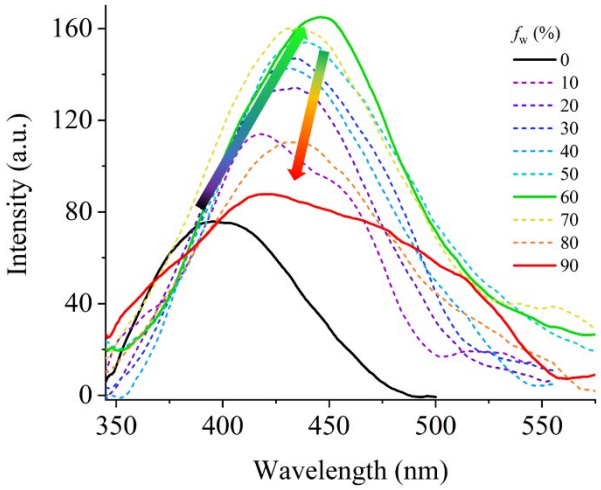

Figure S5. Fluorescence emission spectra of **2** in THF/H_2O mixtures with different f_w.

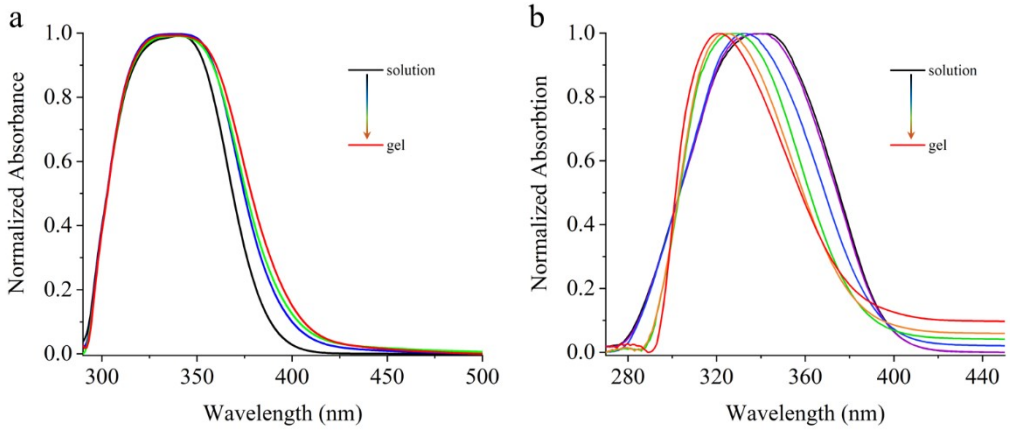

Figure S6. Time-dependent UV-vis absorption spectra for **2** (a) and **1** (b) in acetone/H_2O (v/v=1/1, 5 mg mL^{-1} for both) upon aging the pre-sonicated hot solutions to room temperature.

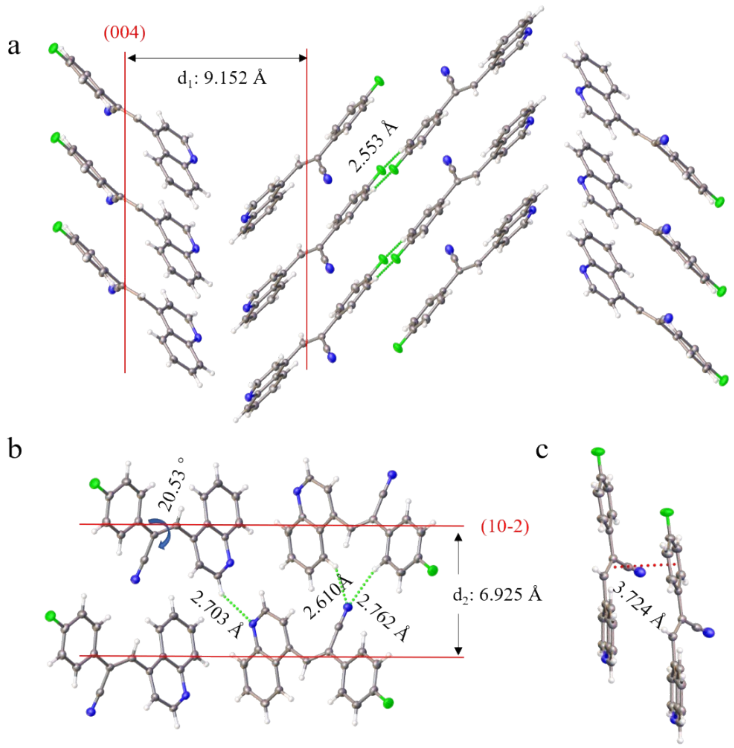

Figure S7. (a) The single crystal structure of **2** viewed along the a-axis and the distance of C–H···F interactions between two adjacent molecules; (b) the dihedral angle between the plane of the phenyl and quinolyl ring and the distance of C–H···N interactions; (c) the distance of p-π conjugate. The red lines refer to the Miller planes.

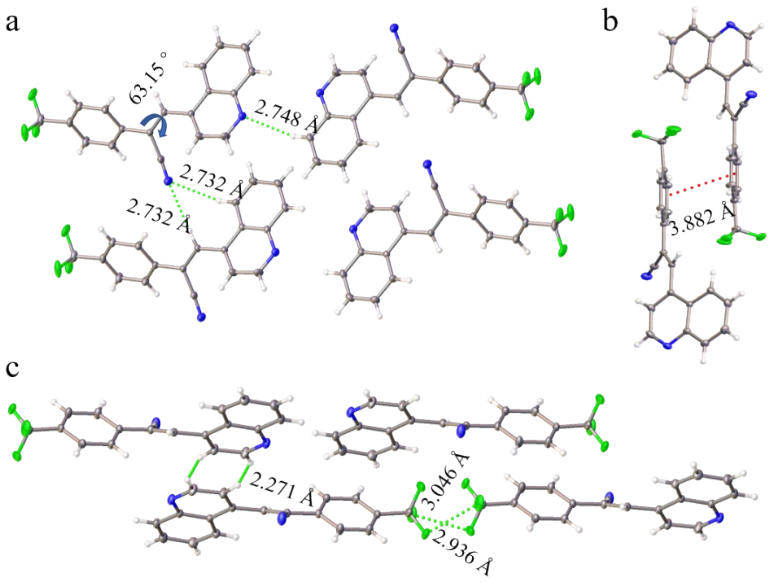

Figure S8. (a) The dihedral angle between the plane of the phenyl and quinolyl ring and the distance of C–H···N interactions in the single crystal of **3**; (b) the distance between two adjacent parallel benzene rings; (c) the single crystal structure viewed along the a-axis and the distance of the H···H interactions as well as the F···F interactions.

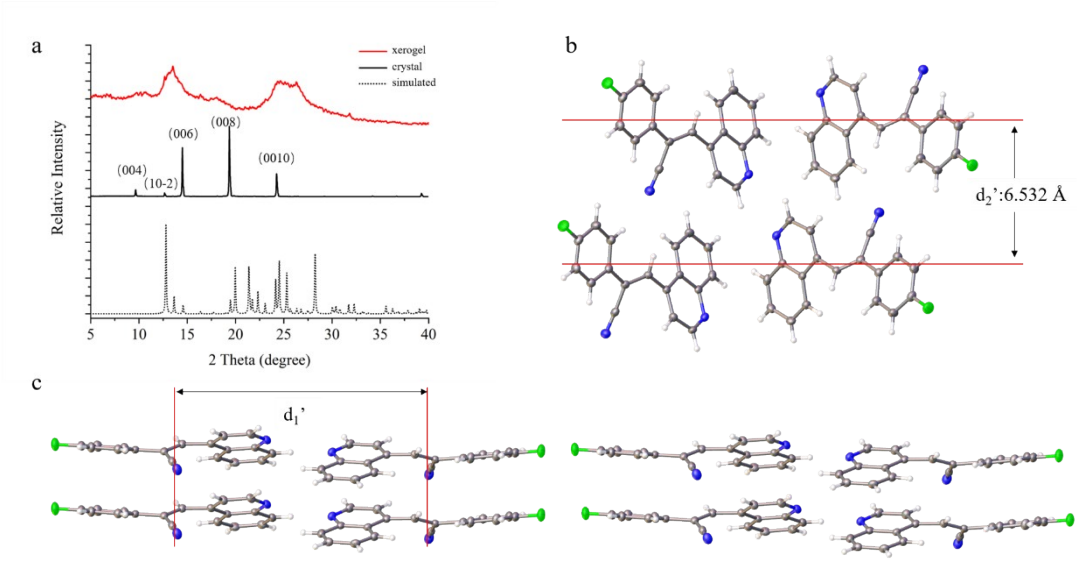

Figure S9. (a) PXRD patterns of **2** in xerogels and crystals, as well as the simulated PXRD pattern from single crystal structure of **2** (b,c). The possible crystal packing of **2** in xerogels. The diffraction peaks of microcrystals of **2** (black) at 9.69°, 14.52°, 19.45° and 24.29° are attributed to (004), (006), (008) and (0010) Miller planes, respectively. These miller planes are parallel to the dominant faces of crystal with d value of 9.152 Å (d_1 in Figure S7). The diffraction peak at 12.68° is corresponding to (10-2) Miller plane with d value of 6.925 Å (d_2 in Figure S7).

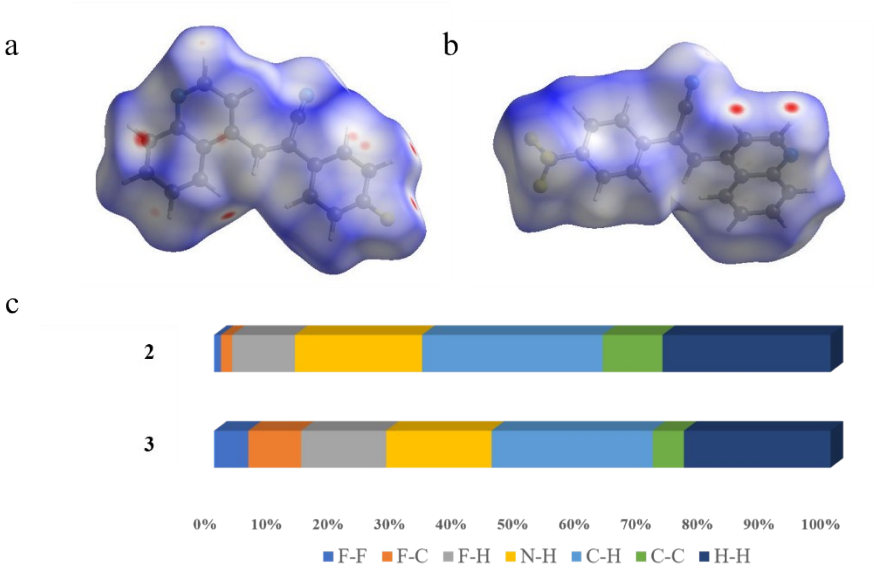

Figure S10. The Hirshfeld surface of an individual molecule in crystals of **2** (a) and **3** (b), relative contributions of various contacts to the Hirshfeld surface of **2** and **3** (c).

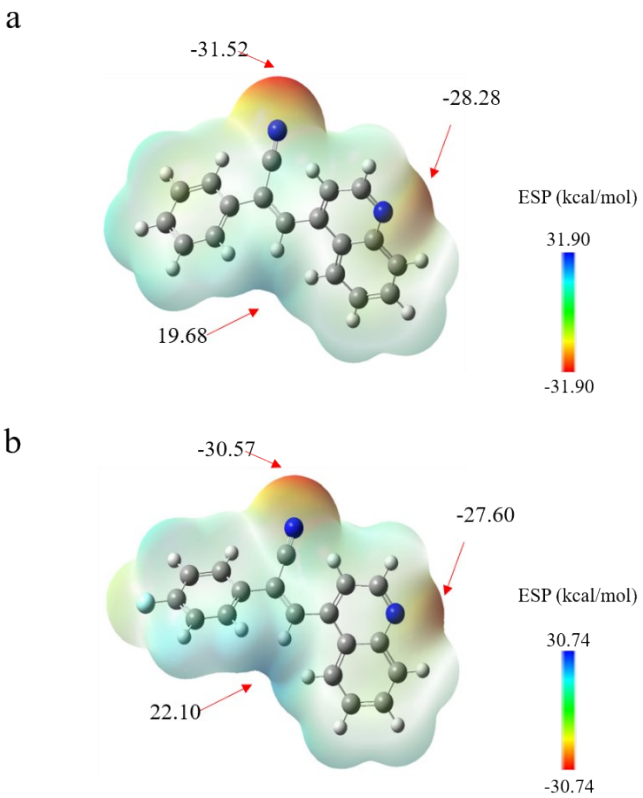

Figure S11. 3D representation of the electrostatic potentials isosurface of **1** (a) and **2** (b) mapped onto its total density surface, determined using DFT at the B3LYP/6-31G(d) level. The units are in kcal/mol.

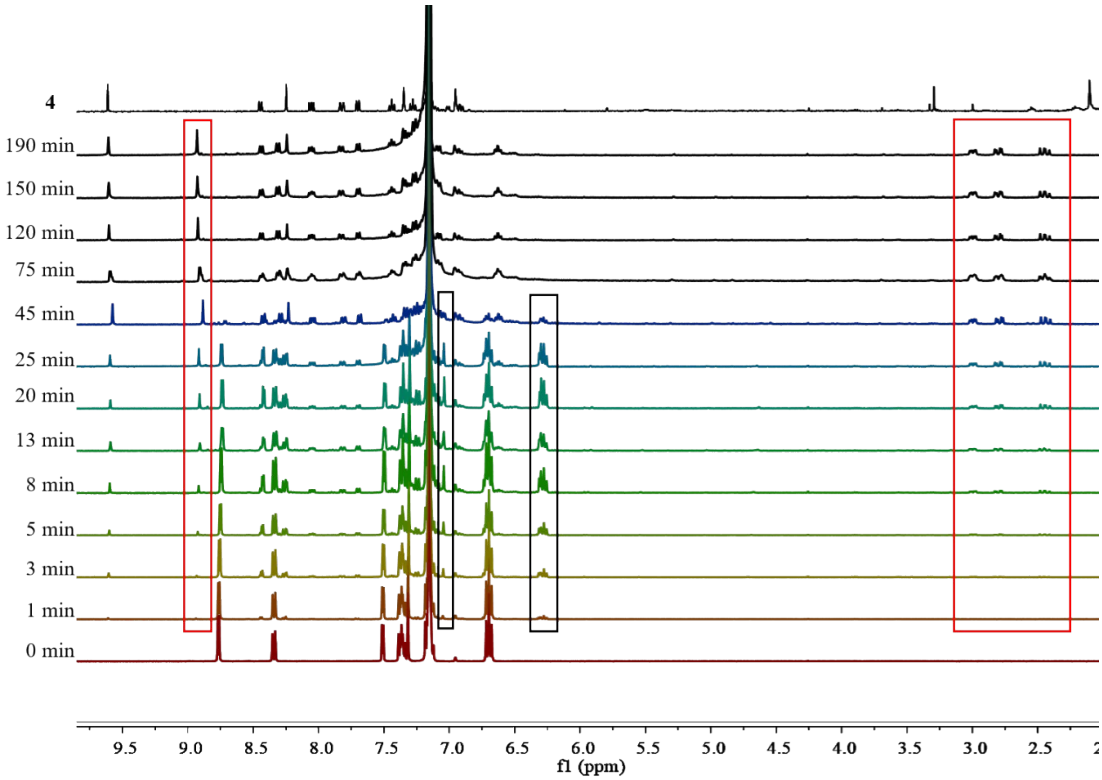

Figure S12. ^{1}H NMR spectra of **2** before and after irradiation by 365 nm light (16.7 mW/cm^2) for different times in benzene-d_6; and ^{1}H NMR spectra of **4**. The red and black boxes show the newly emerged signals during photoreaction.

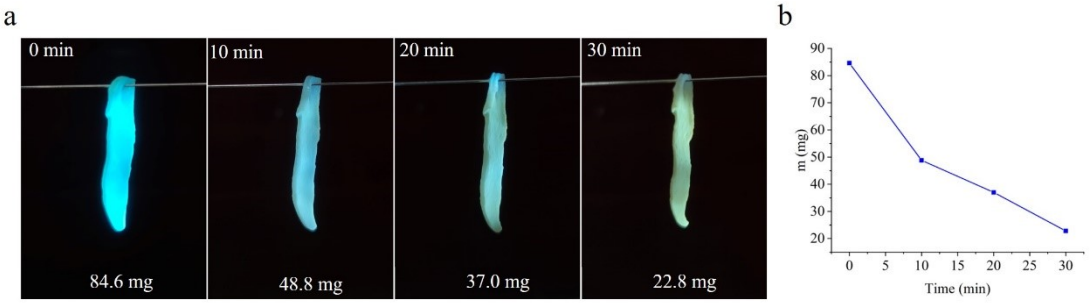

Figure S13. (a) Photos of FSOG of **2** (0.74 wt%, $v_{acetone}/v_{water}$ = 1/1) exposing to 365 nm light (16.7 mW/cm^2) for different times; (b) The mass of FSOG of **2** after irradiation with 365 nm light (16.7 mW/cm^2) for different times.

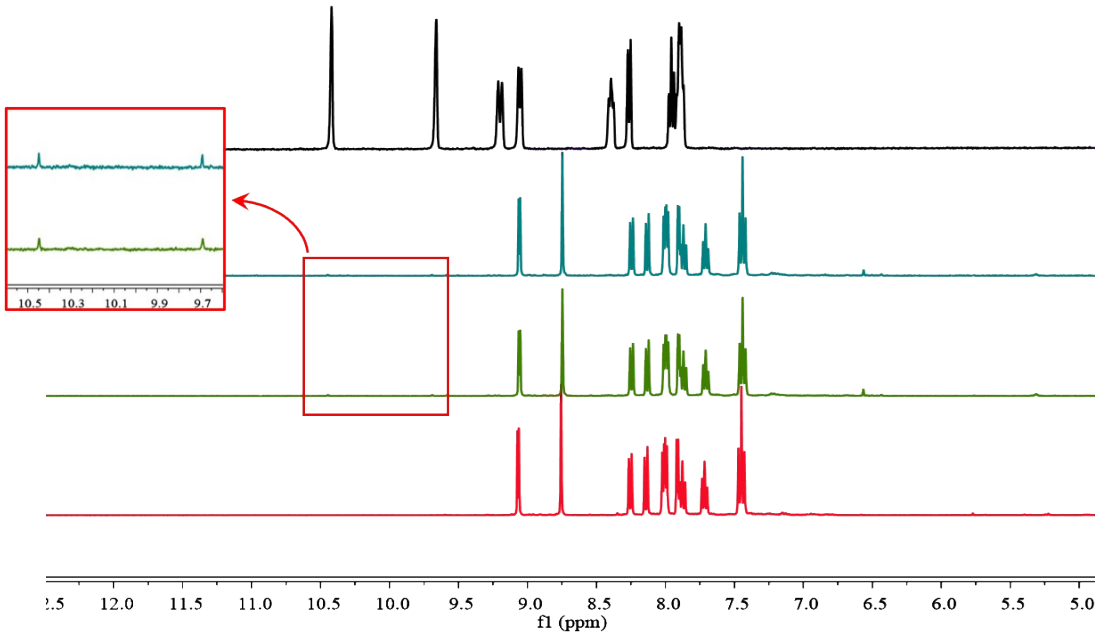

Figure S14. ^{1}H NMR spectra of **2** before (red) and after irradiating its FSHG (FSOG: 0.74 wt%, $v_{acetone}/v_{water}$ = 1/1, green) and FSOG (0.74 wt%, $v_{acetone}/v_{water}$ = 1/1, blue) by 365 nm light (16.7 mW/cm^2) for 30 min, followed by dissolved in DMSO-d_6; and ^{1}H NMR spectra of **4** (black). The red and black boxes show the newly emerged signals during photoreaction.

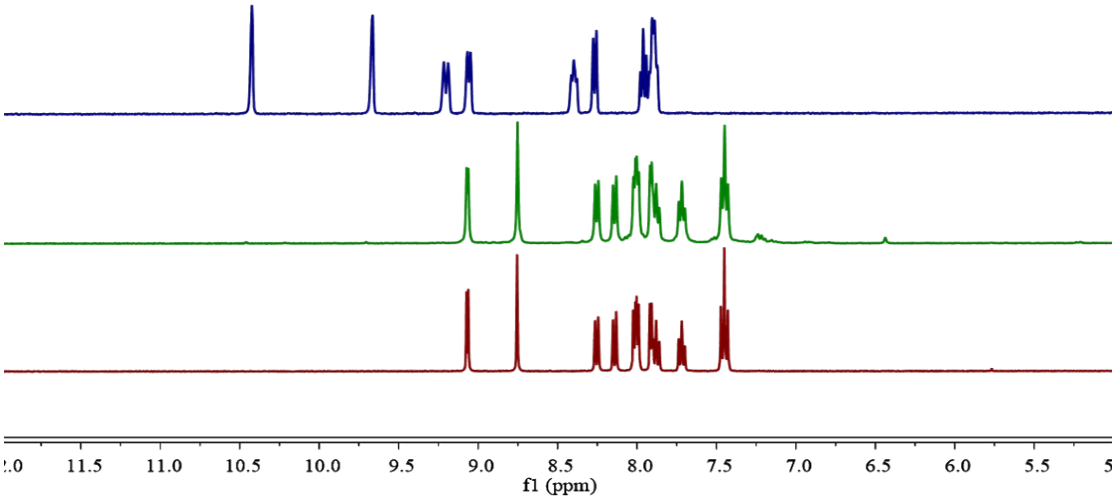

Figure S15. ^{1}H NMR spectra of **2** before (red) and after (green) irradiation by 365 nm light (16.7 mW/cm^2) for 40 min in xerogel, followed by dissolved in DMSO-d_6; and ^{1}H NMR spectra of **4** (blue).

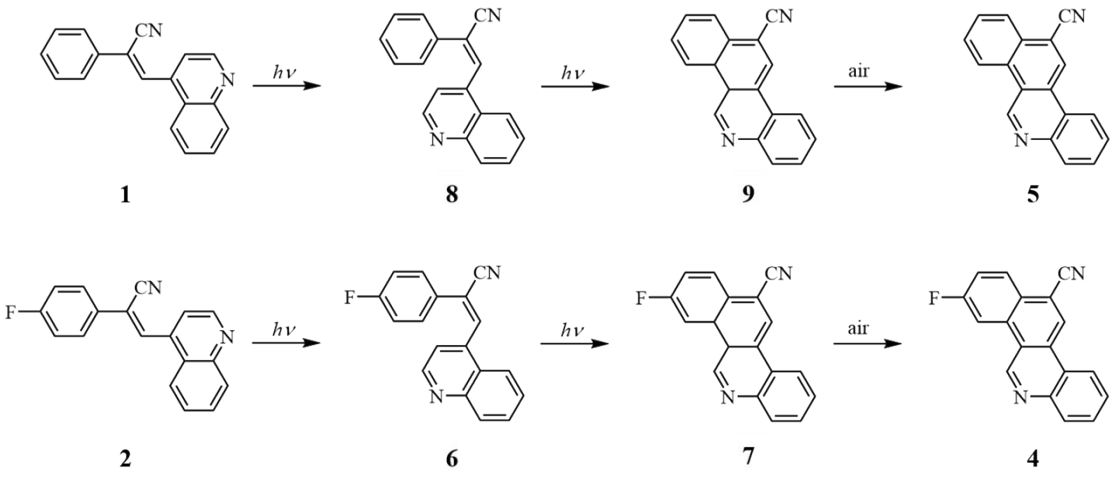

Scheme S1. The photo-induced transformation from **2** to **4**, and from **1** to **5**.[1]

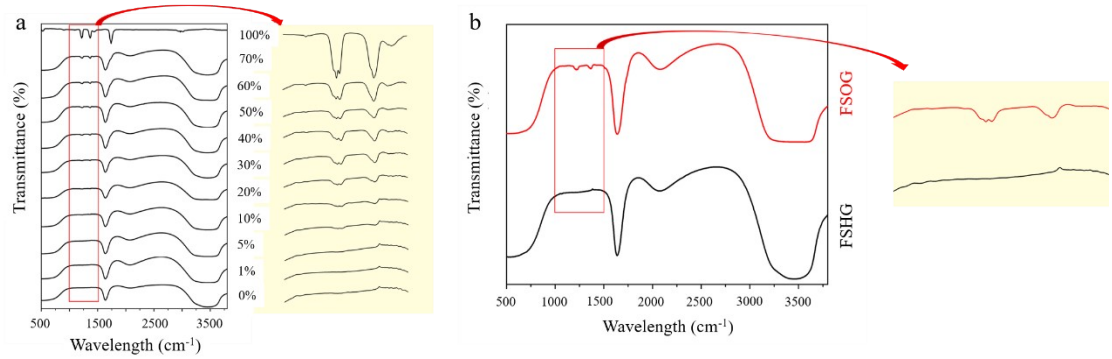

Figure S16. (a) the Fourier transform infrared spectra (FTIR) standard card of acetone/H_2O with different fraction of acetone. (b) the FTIR of solvent in FSOG and FSHG.

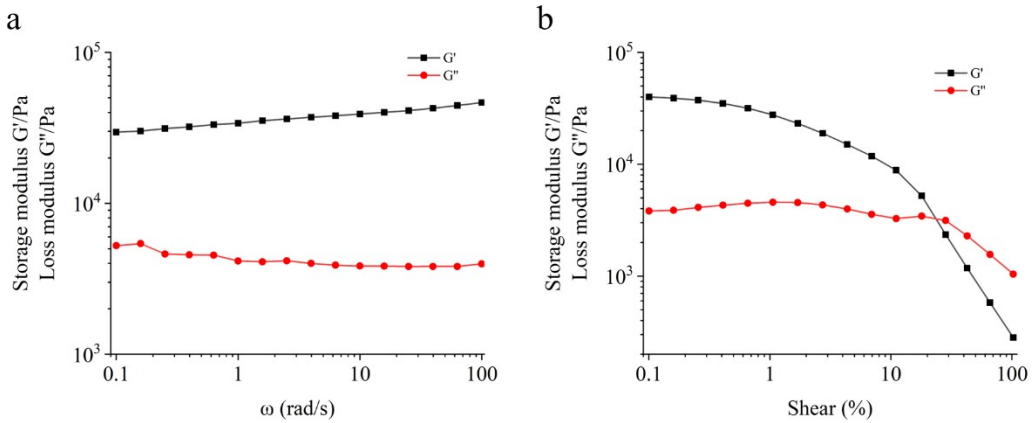

Figure S17. (a) Frequency dependence of storage modulus (G′) and loss modulus (G″) of FSHG based on **2** (FSOG: 0.74 wt%, $v_{acetone}/v_{water}$ = 1/1, strain: 0.1%); (b) Shear dependence of G′ and G″ of FSHG based on **2** (FSOG: 0.74 wt%, $v_{acetone}/v_{water}$ = 1/1, angular frequency at 5 rad/s).

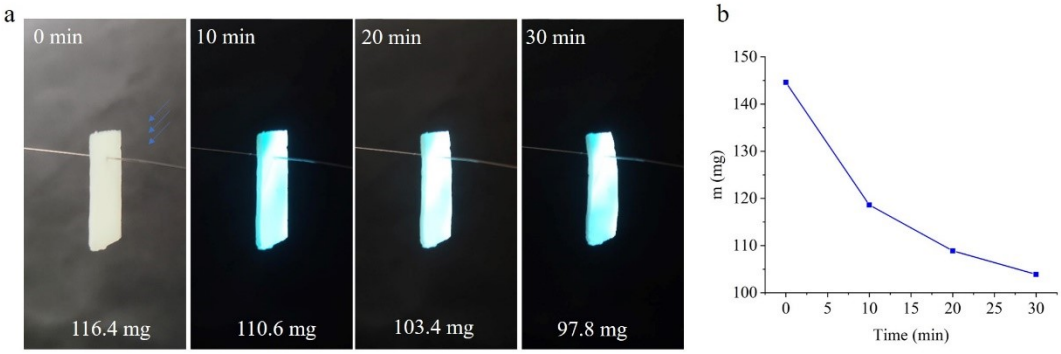

Figure S18. a) Photos of FSHG based on **2** (FSOG: 0.74 wt%, $v_{acetone}/v_{water}$ = 1/1) exposing to 365 nm light (16.7 mW/cm^2) for different times. b) The mass of FSHG based on **2** after irradiation with 365 nm light (16.7 mW/cm^2) for different times.

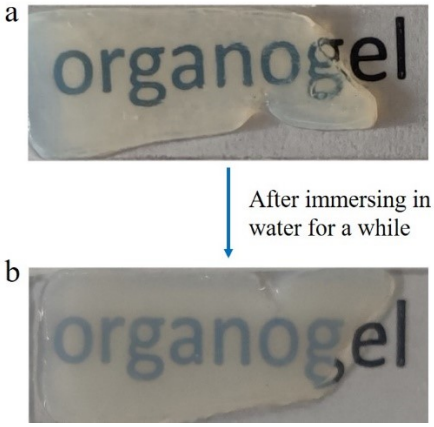

Figure S19. Photos of FSOG of **2** before (a) and after (b) water treatment.

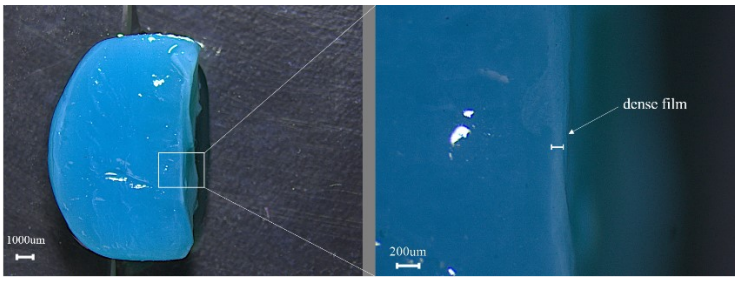

Figure S20. Microscopy photos of cross section of FSHG based on **2**.

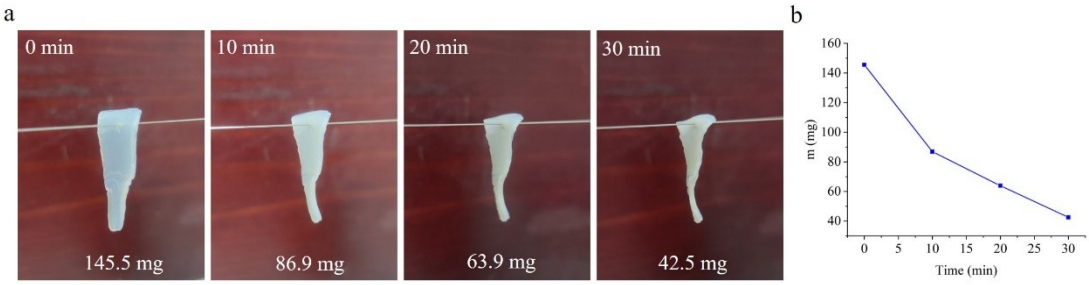

Figure S21. (a) Photos of FSOG based on **2** (0.74 wt%, $v_{acetone}/v_{water}$ = 1/1) exposing in air for different times. (b) The time-dependent mass of FSOG based on **2**.

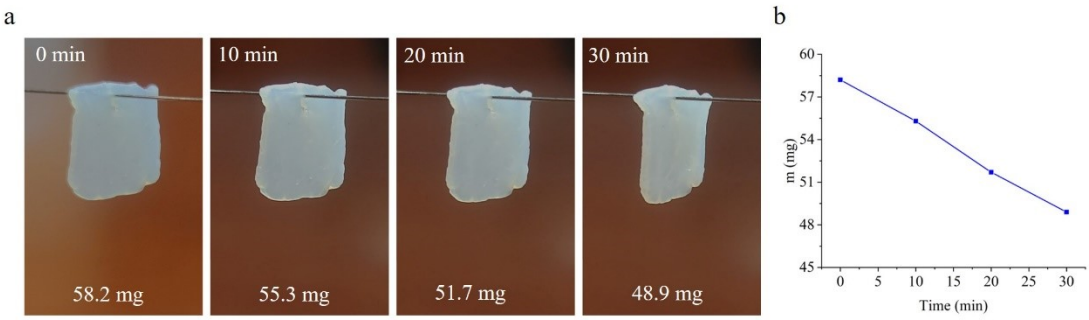

Figure S22. (a) Photos of FSHG based on **2** (FSOG: 0.74 wt%, $v_{acetone}/v_{water}$ = 1/1) exposing in air for different times; (b) The time-dependent mass of FSHG based on **2**.

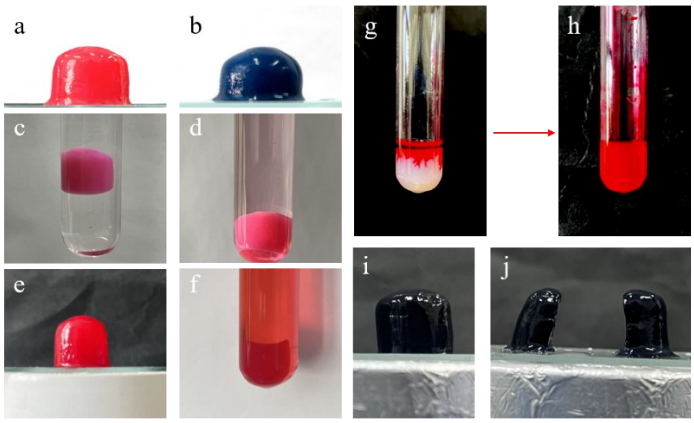

Figure S23. Photos of the FSOG based on **2** after adsorbing Eosin b (a) and Malachite green (b); photos of the FSHG based on **2** containing Eosin b before (c) and after immersing in water for a few days (d); photos of the newly obtained FSOG based on **2** containing Eosin b before (e) and after immersing in water for a few days (f); photos of FSOG based on **2** before (g) and after completely adsorbing Eosin b (h); photos of the FSOG based on **2** that adsorbed ink before (i) and after being cut into two pieces (j).

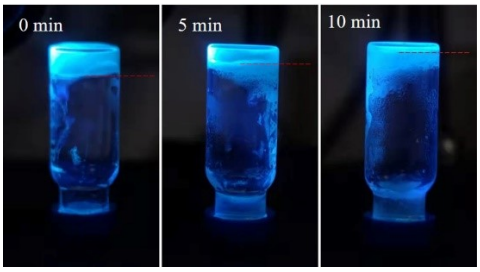

Figure S24. Photos of the organogel based on **1** collapse under irradiation by 365 nm light for different times.

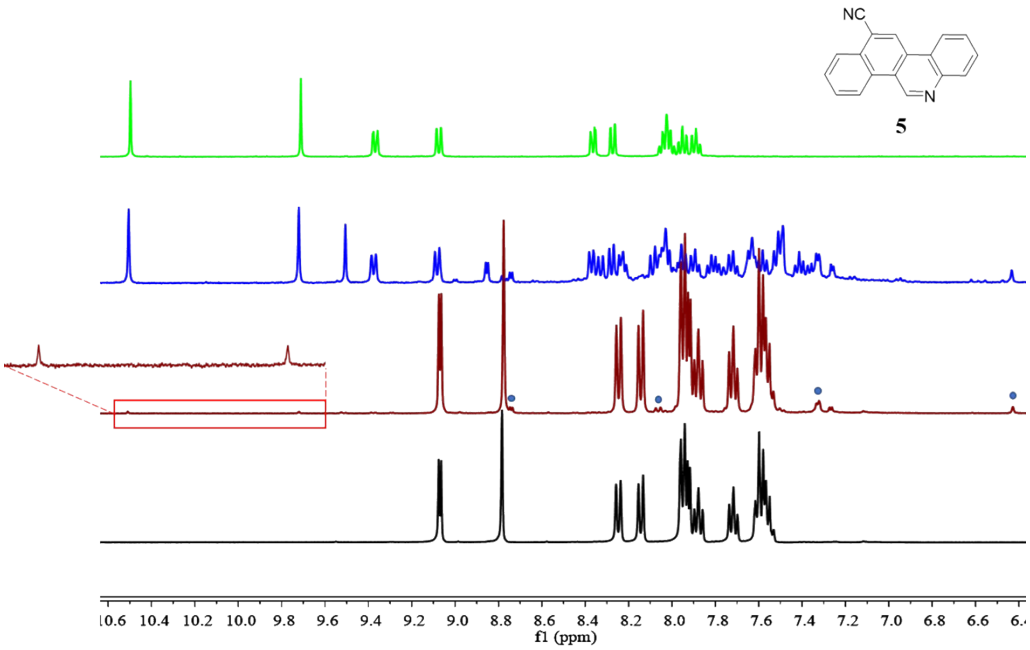

Figure S25. ^{1}H NMR spectra of **1** before (black) and after irradiating xerogel (red) with 365 nm light (16.7 mW/cm^2) for 30 min, followed by dissolved in DMSO-d_6; and irradiating organogel (blue) for 30 min, followed by dried and then dissolved in DMSO-d_6; and the ^{1}H-NMR spectrum of **5** (green). The blue pots and the red rhombic boxes show the newly emerged signals after isomerization and electrocyclization. Inset: the crystal structure of **5**.

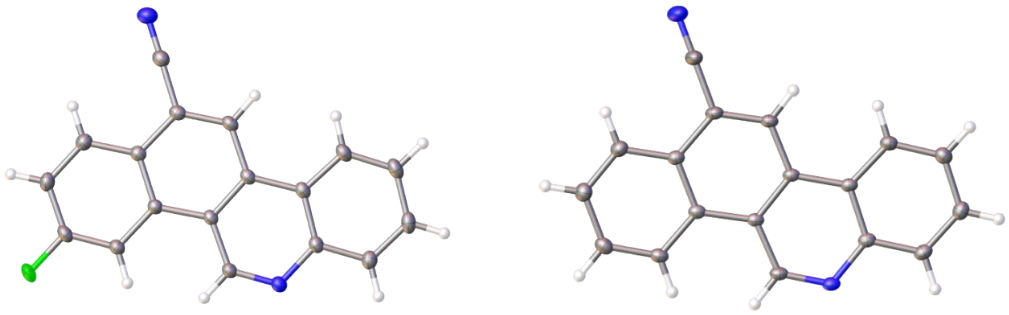

Figure S26. The single crystal structures of **4** (left) and **5** (right).

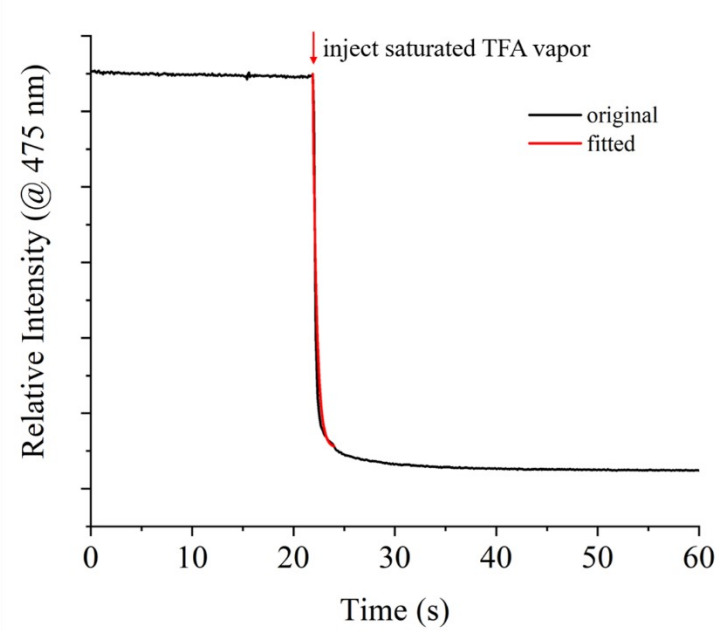

Figure S27. Time-course of fluorescence quenching (λ_{ex} = 350 nm) for the xerogel film of **2** upon exposure to saturated TFA vapor.

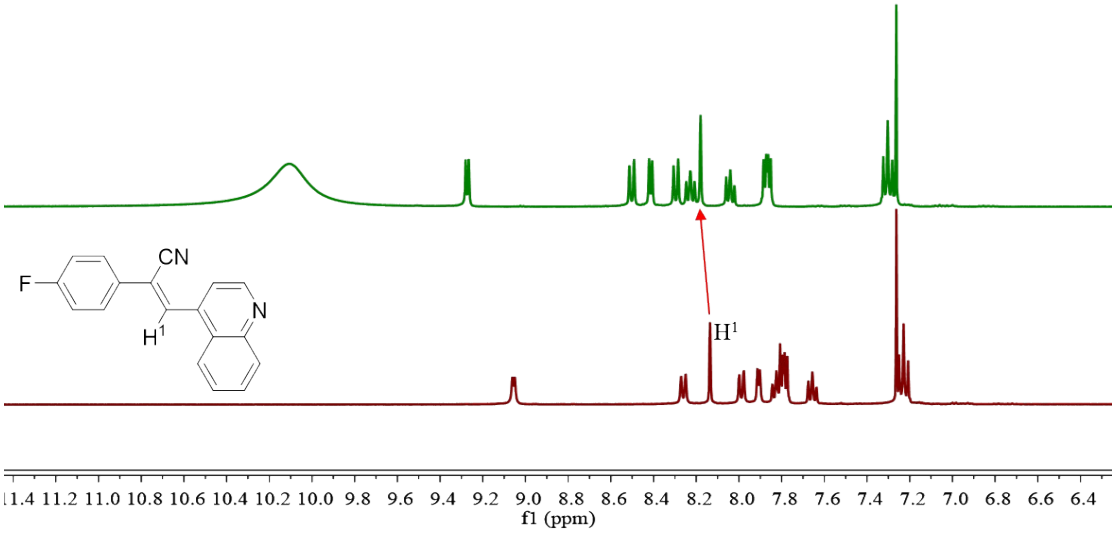

Figure S28. ^{1}H NMR spectra of **2** before (red line) and after adding 10 equiv. (green line) of TFA in $CDCl_3$.

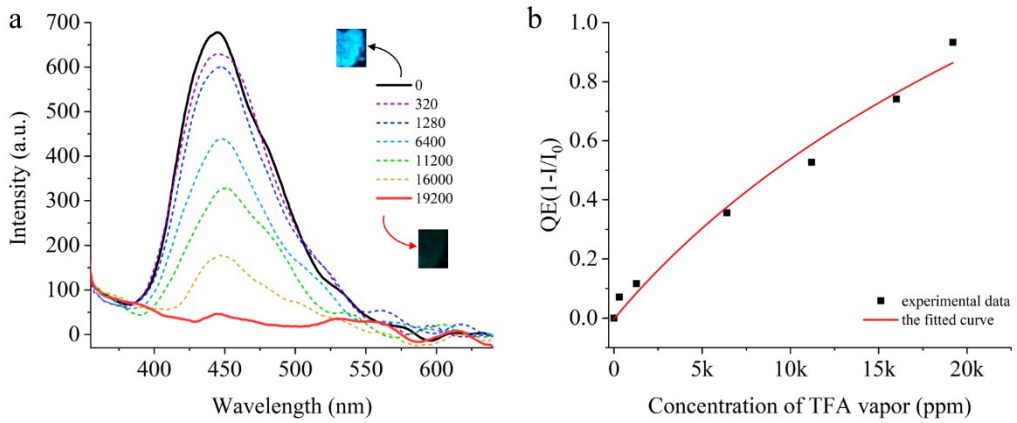

Figure S29. (a) Fluorescence emission spectra of **1** in xerogel film upon exposed to different amount of TFA vapor (0-19200 ppm) (λ_{ex} = 350 nm). Insets: the photos of xerogel film of **1** before and after fuming with TFA vapor (19200 ppm). (b) Concentration-dependent fluorescence quenching efficiency at 447 nm for **1** in xerogel-based film upon exposed to TFA vapor.

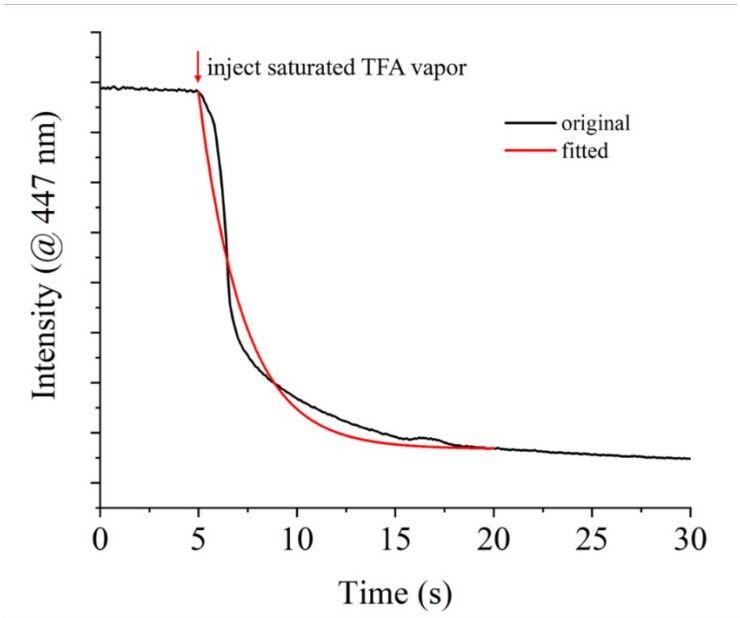

Figure S30. Time-course of fluorescence quenching (λ_{ex} = 350 nm) of the **1** xerogel film upon exposure to saturated TFA vapor.

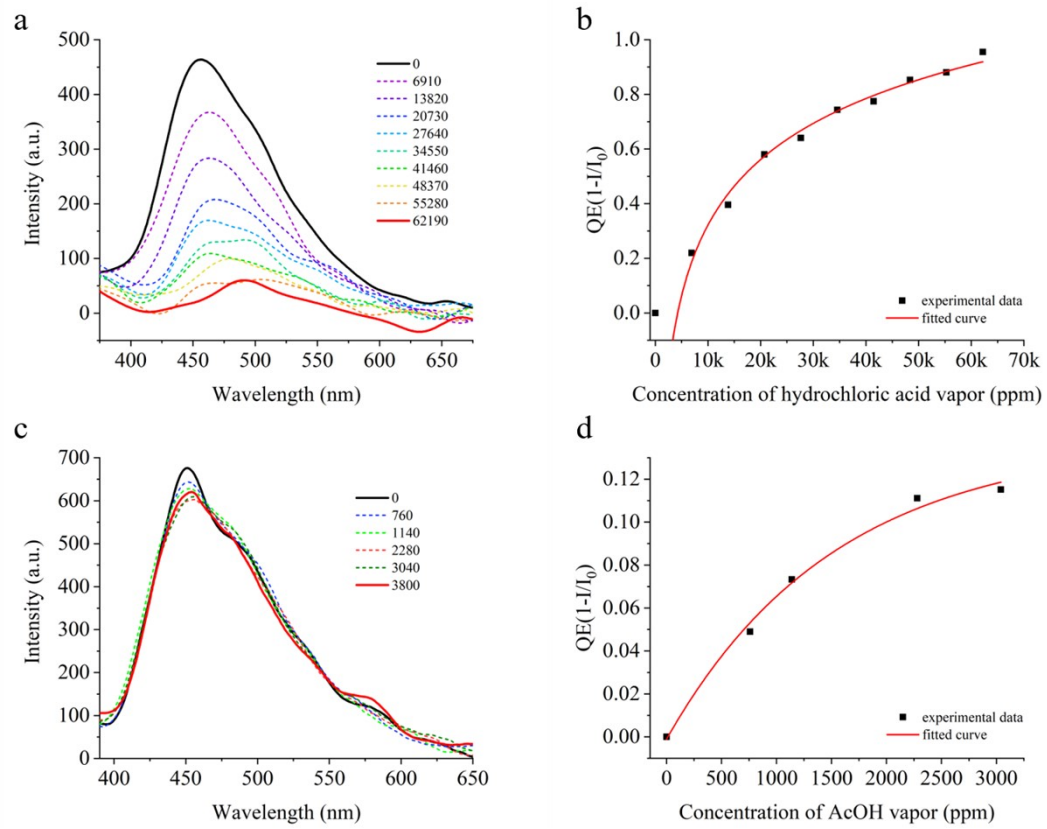

Figure S31. Fluorescence emission spectra of **2** in xerogel film upon exposed to different amount of hydrochloric acid (a) and acetic acid vapor (c, λ_{ex} = 350 nm). Concentration-dependent fluorescence quenching efficiency at 475 nm for **2** in xerogel-based film upon exposed to hydrochloric acid (b) and acetic acid vapor (d).

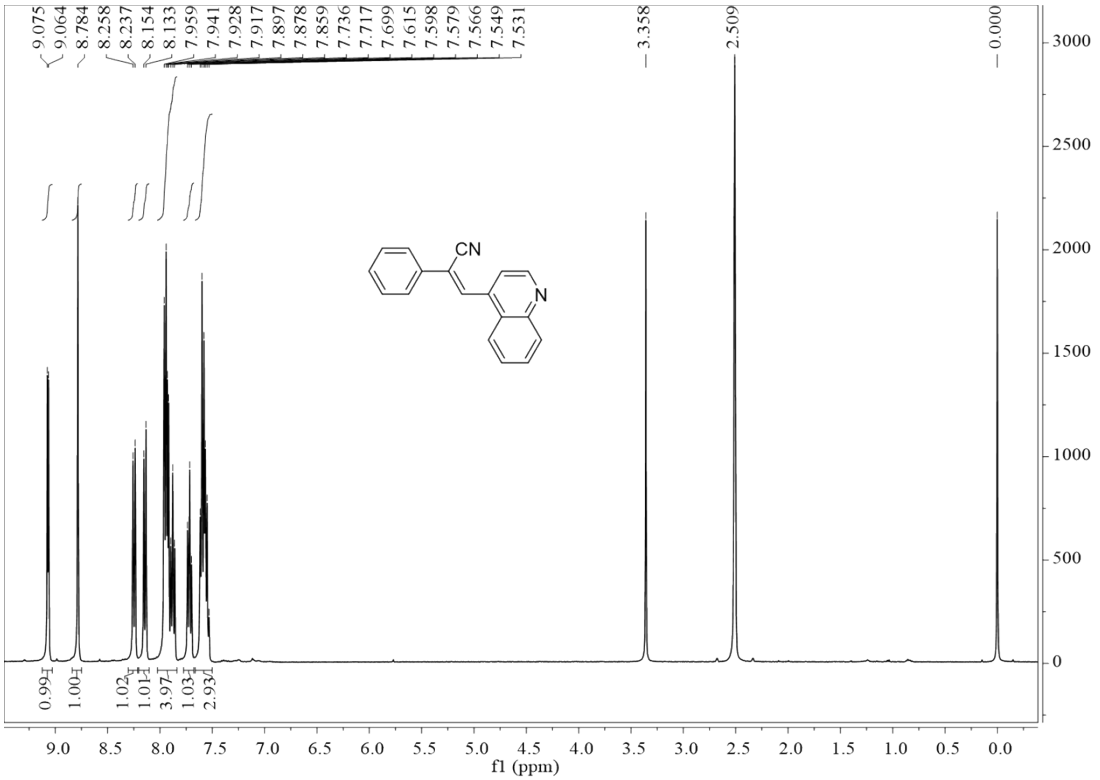

Figure S32. ^{1}H NMR (400 MHz) spectrum of **1** in DMSO-d_6.

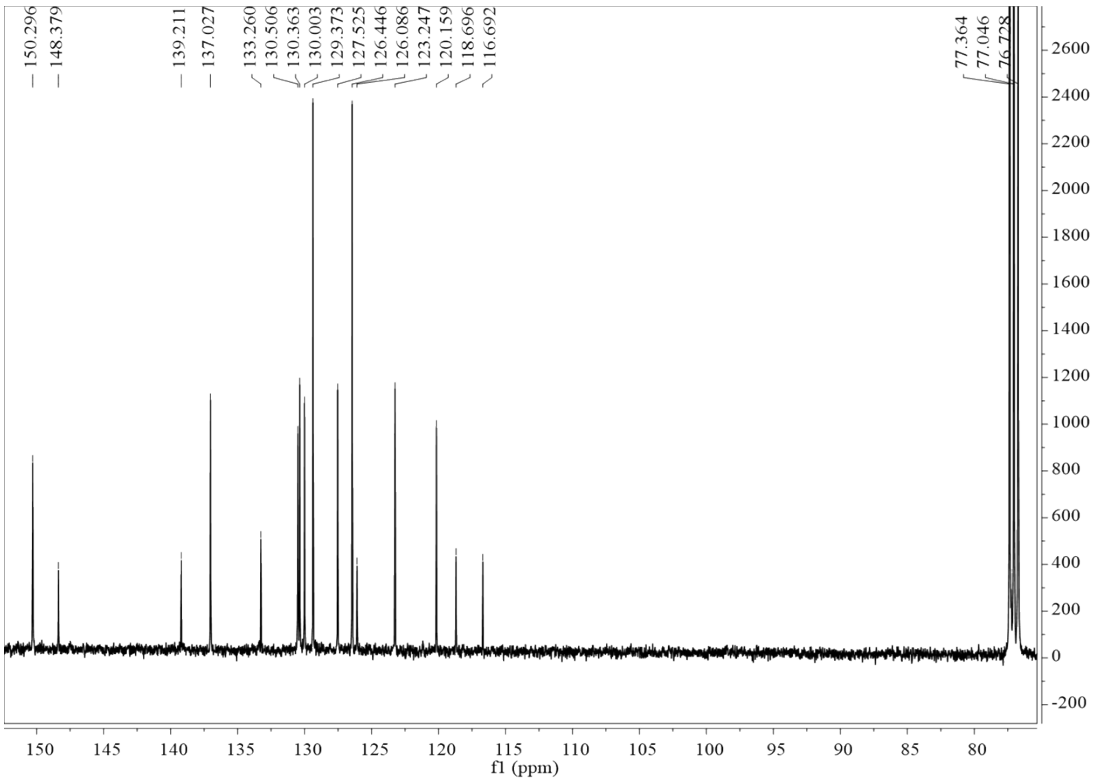

Figure S33. ^{13}C NMR (101 MHz) spectrum of **1** in $CDCl_3$.

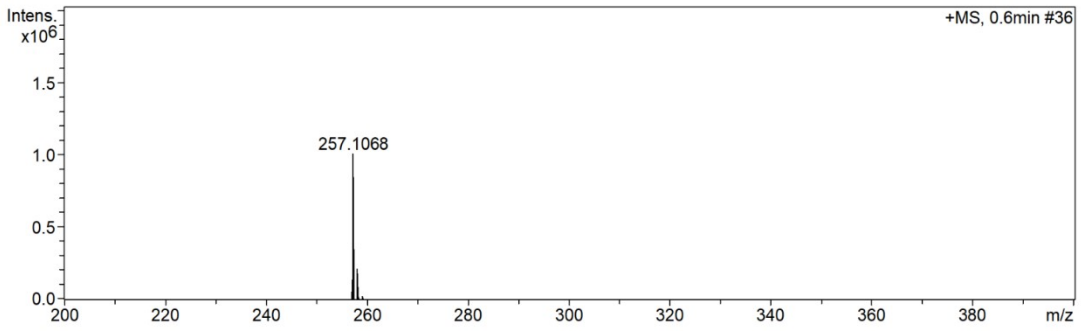

Meas. m/z	#	Formula	m/z	err [ppm]	Mean err [ppm]	rdb	N-Rule	e¡¥Conf	mSigma	Std I	Std Mean m/z	Std I VarNorm	Std m/z Diff	Std Comb Dev
257.1068														
	1	C 18 H 13 N 2	257.1073	1.9	2.7	13.5	ok	even	3.46	0.0065	0.0008	0.0027	0.0009	0.8427

Figure S34. The HRMS spectrum of **1**.

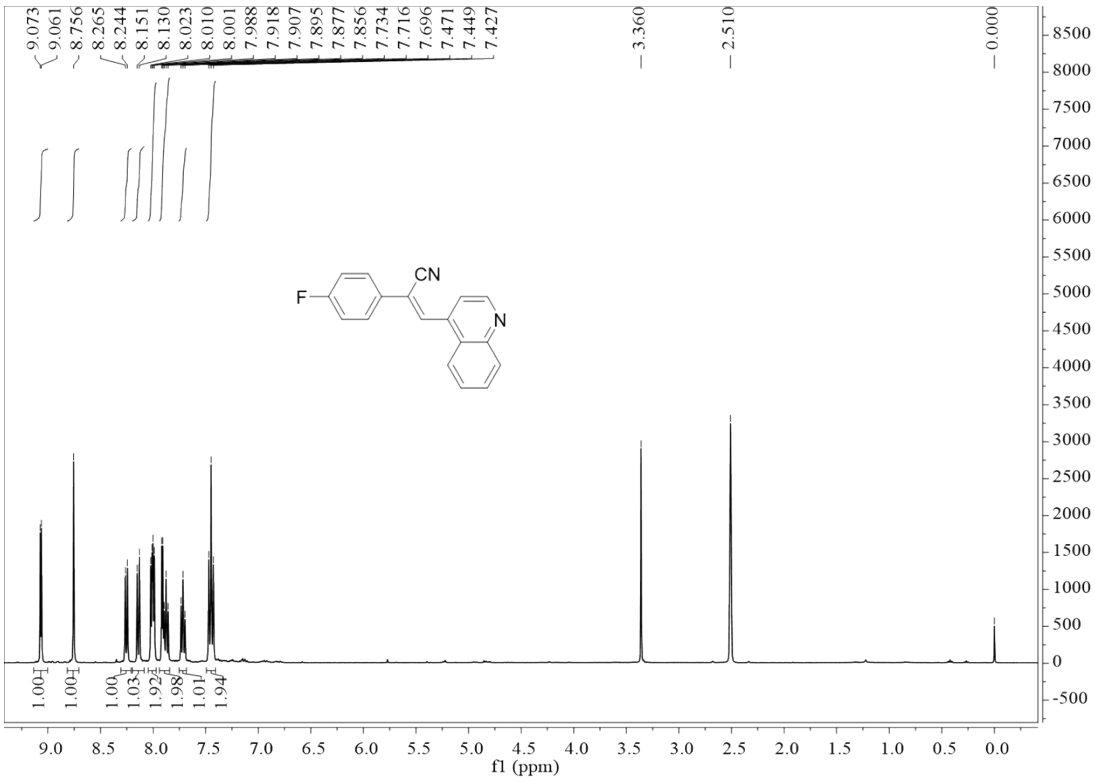

Figure S35. ^{1}H NMR (400 MHz) spectrum of **2** in DMSO-d_6.

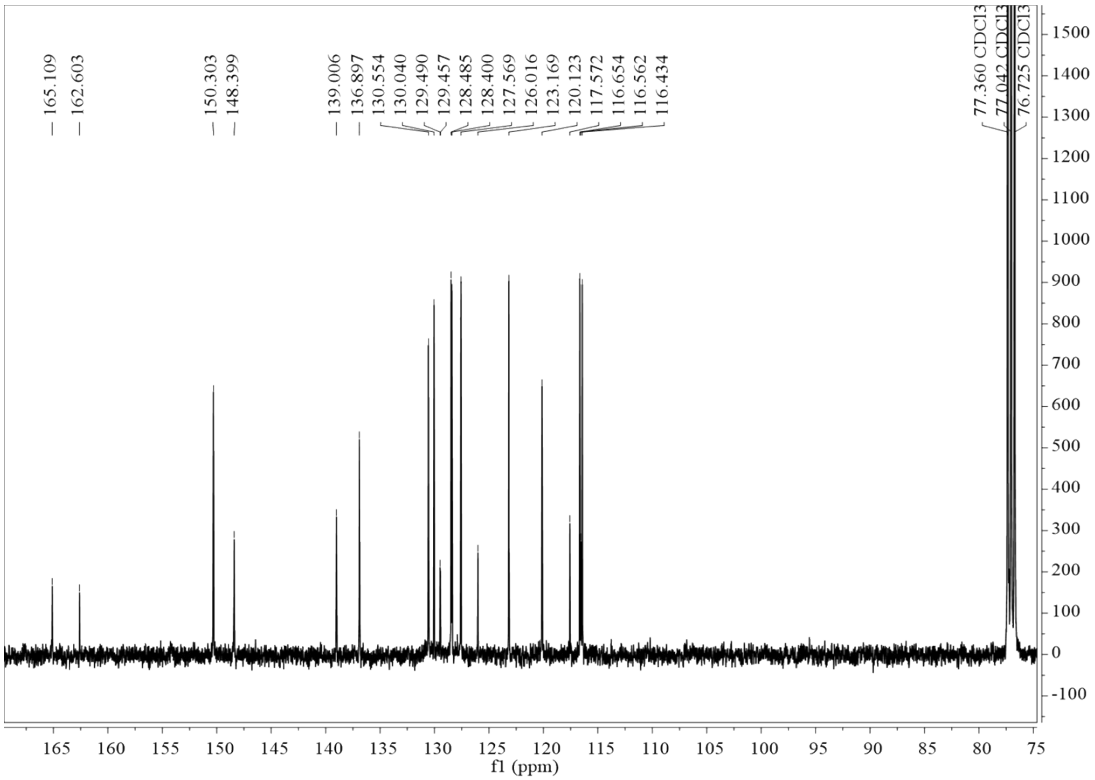

Figure S36. ^{13}C NMR (101 MHz) spectrum of **2** in $CDCl_3$.

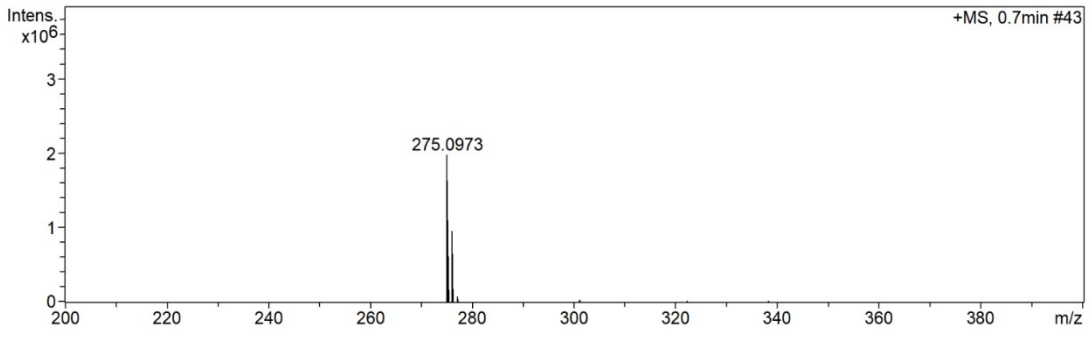

Meas. m/z	#	Formula	m/z	err [ppm]	Mean err [ppm]	rdb	N-Rule	ei¥ Conf	mSigma	Std I	Std Mean m/z	Std I VarNorm	Std m/z Diff	Std Comb Dev
275.0973	1	C 8 H 10 F 3 N 8	275.0975	0.6	-1.7	6.5	ok	even	210.82	0.3182	0.0010	0.1321	0.0019	0.8427

Figure S37. The HRMS spectrum of **2**.

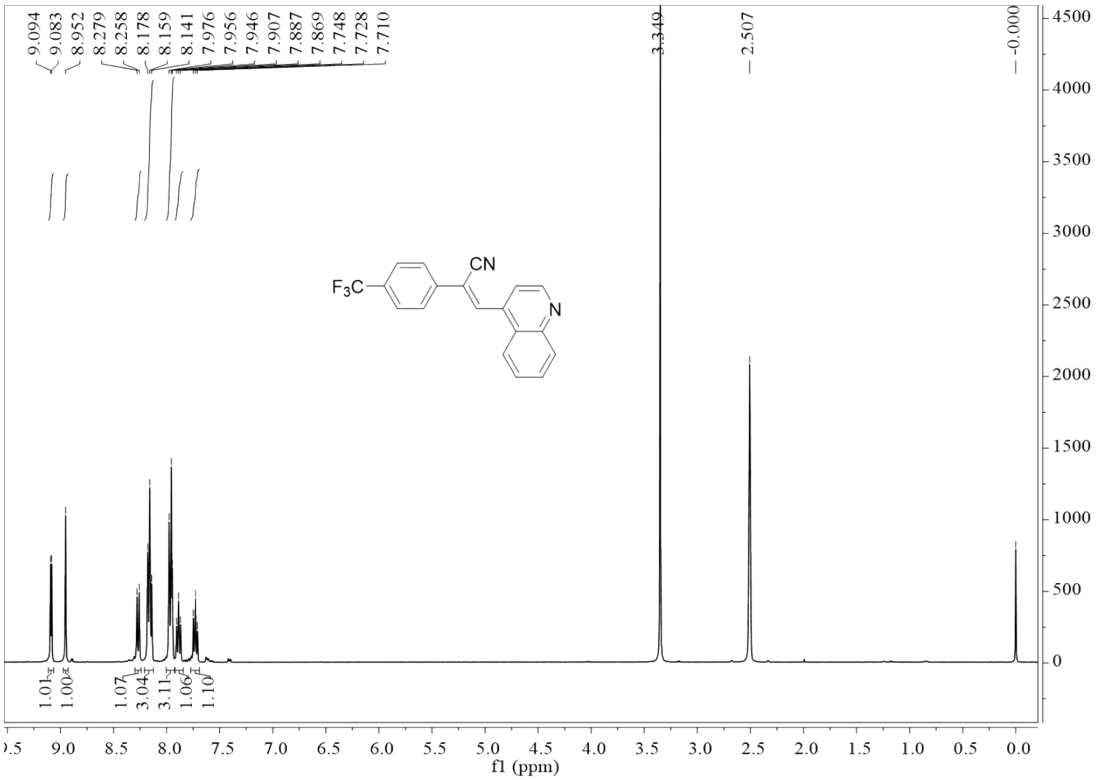

Figure S38. ^{1}H NMR (400 MHz) spectrum of **3** in DMSO-d_6.

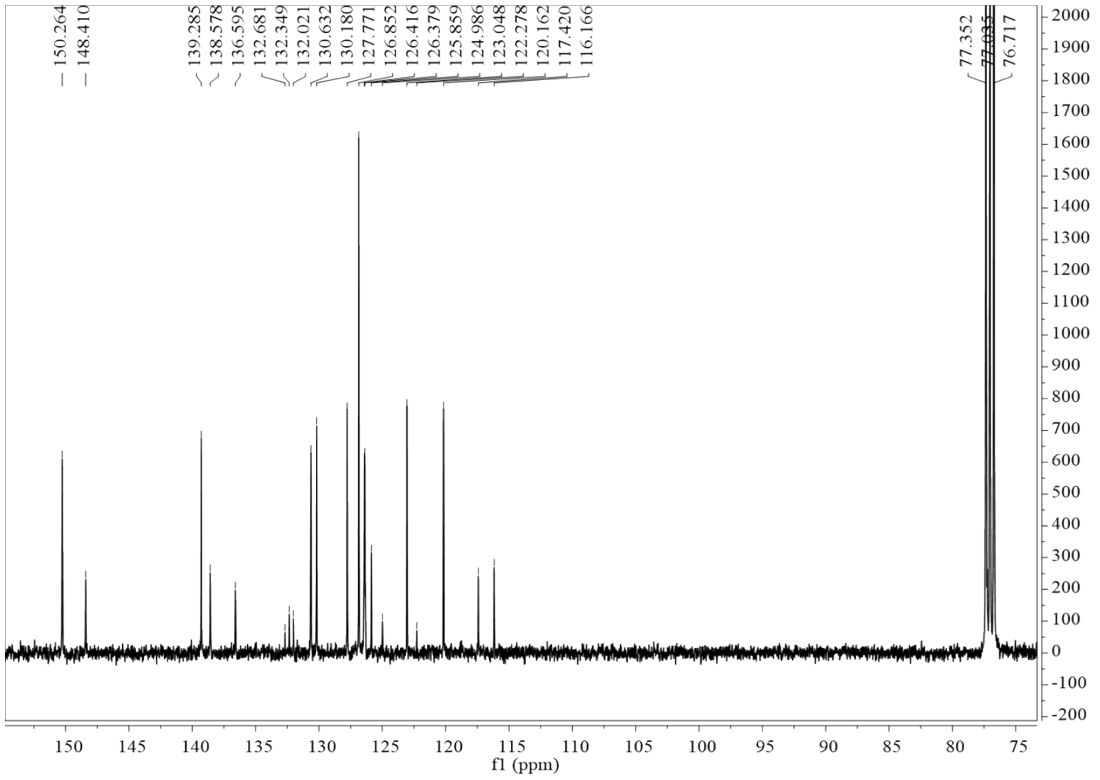

Figure S39. ^{13}C NMR (101 MHz) spectrum of **3** in $CDCl_3$.

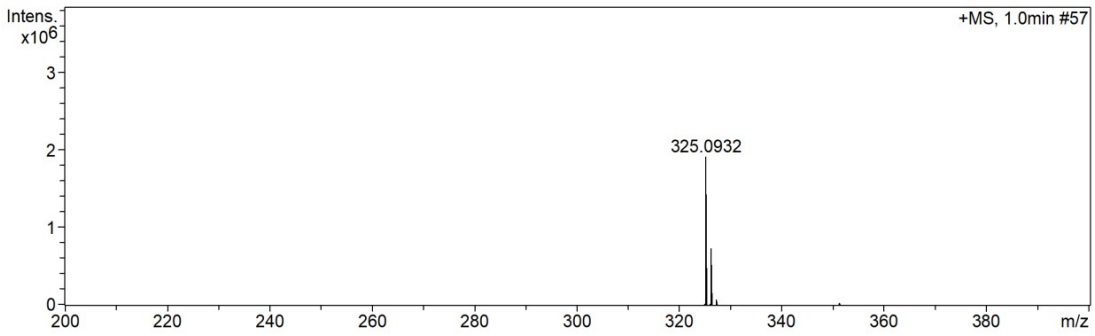

Meas. m/z	#	Formula	m/z	err [ppm]	Mean err [ppm]	rdb	N-Rule	e¡¥Conf	mSigma	Std I	Std Mean m/z	Std I VarNorm	Std m/z Diff	Std Comb Dev
325.0932														
	1	C 19 H 12 F 3 N 2	325.0947	4.7	2.6	13.5	ok	even	99.82	0.1462	0.0014	0.0576	0.0026	0.8427

Figure S40. The HRMS spectrum of **3**.

Reference

1 Sifain A E, Gifford B J, Gao D W, Lystrom L, Nelson T R, Tretiak S. *J. Phys. Chem. A*, 2018, **122**, 9403-9411.

2 Xue P, Ding J, Jin M, Lu R, *J. Mater. Chem. C*, 2017, **5**, 5299-5303.

3 Ma Y, Cametti M, Džolić Z, Jiang S. *J. Mater. Chem. C*, 2016, **4**, 10786-10790.